JOURNAL OF SOLID STATE CHEMISTRY 65, 265–271 (1986)

Ionic Conductivity and Crystal Chemistry of Ramsdellite Type Compounds, $Li_{2+x}(Li_xMg_{1-x}Sn_3)O_8$, $0 \leq x \leq 0.5$ and $Li_2Mg_{1-x}Fe_{2x}Sn_{3-x}O_8$, $0 \leq x \leq 1$

J. GRINS

Department of Inorganic Chemistry, Arrhenius Laboratory, University of Stockholm, S-106 91 Stockholm, Sweden

AND A. R. WEST

Department of Chemistry, University of Aberdeen, Meston Walk, Old Aberdeen, AB9 2UE, Scotland, United Kingdom

Received August 21, 1985; in revised form February 5, 1986

Solid solution phases $Li_{2+x}(Li_xMg_{1-x}Sn_3)O_8$: $0 \leq x \leq 0.5$ and $Li_2Mg_{1-x}Fe_{2x}Sn_{3-x}O_8$: $0 \leq x \leq 1$, both with ramsdellite type structure, have been synthesized by solid state reaction at 1773 and 1523 K, respectively. The relationship of the ramsdellite structure to the recently illustrated, tetragonal-packed structure is given. The $Li_{2+x}(Li_xMg_{1-x}Sn_3)O_8$ solid solutions exhibit conductivities 4×10^{-6}–5×10^{-4} $(\Omega\ cm)^{-1}$ at 573 K and corresponding activation energies, 0.93–0.74 eV. The highest conductivity was observed for $Li_{2.3}(Li_{0.3}Mg_{0.7}Sn_3)O_8$, $x = 0.3$. In the solid solution series $Li_2Mg_{1-x}Fe_{2x}Sn_{3-x}O_8$, the highest conductivity was exhibited by $Li_2Fe_2Sn_2O_8$, 2×10^{-5} $(\Omega\ cm)^{-1}$ at 573 K.

Introduction

A number of Li-containing oxides, such as $Li_2Fe_2Sn_2O_8$ (*1*), $Li_2MgSn_3O_8$ (*2*), and $Li_2Ti_3O_7$ (*3*) exhibit crystal structures which can be regarded as derived from the ramsdellite structure. $Li_2Ti_3O_7$ has been found to be a fairly good Li^+ ion conductor with an activation energy $E_a = 0.46$ eV (*4*, *5*). In order to investigate whether other ramsdellite type compounds exhibit similar solid electrolyte properties, a series of materials with ramsdellite type structures have been synthesized and their ionic conductivities determined.

The Ramsdellite Structure

Ramsdellite, one of the modifications of MnO_2, possesses an orthorhombic crystal structure with space group *Pbnm* (*6*, *7*). An illustration of an idealized undistorted (see below) ramsdellite structure is given in Fig. 1b in projection down the *c*-axis. This MO_2 structure contains MO_6 octahedra linked by sharing edges to form infinite double columns extending in the *c* direction. The double columns are linked via their corners with adjacent double columns to form a framework containing channels along the *c*-axis. The channel sites are empty in MnO_2.

0022-4596/86 $3.00

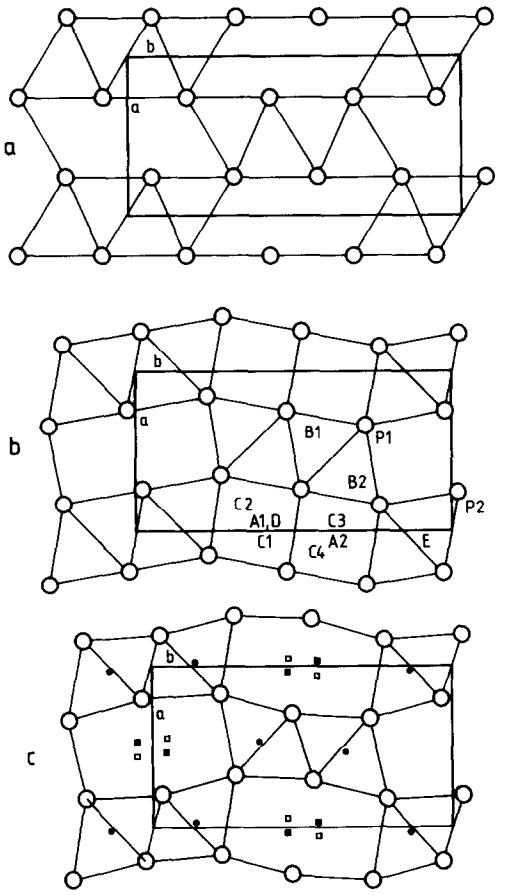

FIG. 1. An [001] projection of the ramsdellite structure. Open circles represent oxygens. (a) A distorted ramsdellite structure with the oxygens in h.c.p. (b) An ideal "tetragonal-packed" ramsdellite structure. (c) The $Li_2Ti_3O_7$ structure (*3*). The positions of the Li^+ ions in the channels are illustrated (□ and ■).

The Li-containing oxides of concern here possess ramsdellite derivative structures in which all or part of the Li^+ ions occupy sites within the ramsdellite channels. In $Li_2Ti_3O_7$, both TiO_6 and LiO_6 octahedra constitute the framework, together with extra Li^+ ions in the channels and the formula of $Li_2Ti_3O_7$ may accordingly be written as $Li^c_{2/7}(Li_{4/7}Ti_{24/7})^fO_8$ where c and f refer to channel and framework sites, respectively.

The ramsdellite structure is also commonly described as containing a distorted h.c.p. array of oxygen with half of the octahedral sites occupied by the metal ions, *M*. A ramsdellite structure in which the oxide ions are flattened so as to be ideally h.c.p. is shown in Fig. 1a.

The alternative way of describing the ramsdellite structure is obtained by noting the similarity of the oxygen arrangement to that in tetragonal-packed (t.p.) structures (*8*). An ideal ramsdellite structure is accordingly obtained as shown in Fig. 1b, in projection along the *c*-axis. The coordinates of the positions of various sites in space group *Pbnm* are given in Table I. In order to facilitate a comparison of different sites the shortest distance between oxygen ions, equal to the length of an MO_6 octahedron edge, may be set to unity. On this basis the unit cell axes are $a = (\sqrt{2}/2)(1 + \sqrt{2})$, $b = \sqrt{2}(1 + \sqrt{2})$, and $c = 1$. The packing efficiency of the oxygens, as for tetragonal packing, is 71.87% which compares with 74.05% in a h.c.p. array.

The P1 and P2 oxygen ions are each 11-coordinated by oxygens at a distance of 1 with two next-nearest oxygens at a distance of 1.2247. The coordination polyhedra are, however, different and are shown in Fig. 2. The P1 oxygens are coordinated by 11 oxygens as in a tetragonal-packed oxygen ar-

TABLE I

COORDINATES OF POSITIONS IN THE "IDEAL" RAMSDELLITE UNIT CELL (SPACE GROUP *Pbnm*)

Position	Wyckoff notation		Coordinates
Oxygen atom	P1	4c	$x,y,\frac{1}{4}$; $x = 0.6642$, $y = 0.2714$
Oxygen atom	P2	4c	$x,y,\frac{1}{4}$; $x = 0.2500$, $y = -0.0214$
Octahedral site	E	4c	$x,y,\frac{1}{4}$; $x = -0.0429$, $y = 0.1250$
Tetrahedral site	B1	4c	$x,y,\frac{1}{4}$; $x = 0.6036$, $y = 0.4482$
Tetrahedral site	B2	4c	$x,y,\frac{1}{4}$; $x = 0.3107$, $y = 0.3018$
Dist. oct. site	A1	4c	$x,y,\frac{1}{4}$; $x = 0.0429$, $y = 0.6250$
Dist. oct. site	A2	4c	$x,y,\frac{1}{4}$; $x = -0.0429$, $y = 0.3750$
Dist. tet. site	D	8d	x,y,z; $x = 0.0429$, $y = 0.6250$, $z = 0$.
Dist. tet. site	C1	4c	$x,y,\frac{1}{4}$; $x = -0.0547$, $y = 0.5905$
Dist. tet. site	C2	4c	$x,y,\frac{1}{4}$; $x = 0.1405$, $y = 0.6595$
Dist. tet. site	C3	4c	$x,y,\frac{1}{4}$; $x = 0.0261$, $y = 0.3262$
Dist. tet. site	C4	4c	$x,y,\frac{1}{4}$; $x = -0.1119$, $y = 0.4238$

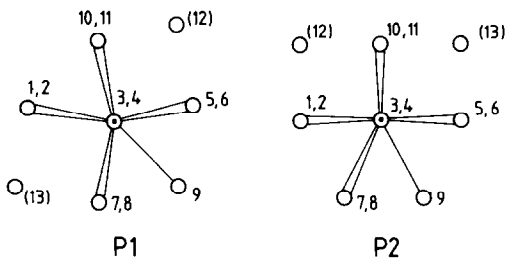

FIG. 2. The oxygen arrangement around the P1 and P2 oxygen atoms.

ray. The P2 oxygens have six nearest neighbors in a plane parallel with the double columns, three in a parallel plane below, and two in a parallel plane above.

The M ions are located in the undistorted octahedral sites E with six oxygens at a distance of 0.7071 (Fig. 1b). There are undistorted tetrahedral sites, B1 and B2, located in the double columns of MO_6 octahedra with a distance to oxygen of 0.6123. In the middle of each half of the rectangular channels, there are distorted octahedral sites, A1 and A2, coordinated by four coplanar oxygens at a distance of 0.7906 and two axial oxygens at a distance of 0.6123. Between the A1 and A2 sites there are distorted tetrahedral sites, D, with oxygens at a distance of 0.6614. There are other distorted tetrahedral sites, C1–C4, tetrahedrally arranged around the D sites, each with four oxygens at a distance of 0.6455. As in the case of a tetragonal-packed oxygen array, the number of distorted octahedral and tetrahedral sites in the channels is double the number of equivalent, undistorted sites in a h.c.p. array.

In $Li_2Ti_3O_7$, Fig. 1c, the Li^+ ions in the channels are located at sites corresponding to the distorted tetrahedral sites C1 and C4 of Fig. 1b. The oxygen positions are displaced from the positions shown in Fig. 1b in such a way that the oxygens in the middle of the longer sides of the rectangular channels are pushed apart, thereby widening the channels in the a-direction. As a consequence, the Li–oxygen distances become larger than in the undistorted structure. The possibility of such a distortion occurring may be the reason why the Li-containing oxides of concern here exhibit the ramsdellite structure instead of the tetragonal-packed rutile structure in which a similar distortion is not possible.

For $Li_2Ti_3O_7$ the axial ratios are (*3*) $a/b = 0.526$, $c/a = 0.587$, and for the ramsdellite compounds investigated in this study, $0.510 \leq a/b \leq 0.519$, $0.602 \leq c/a \leq 0.610$, as compared with the axial ratios $a/b = 0.471$, $c/a = 0.612$ for an ideal h.c.p. ramsdellite structure and $a/b = 0.500$, $c/a = 0.586$ for the undistorted ramsdellite structure in Fig. 1b.

Experimental

The materials were prepared by heat treatment of mixtures of appropriate amounts of dried Li_2CO_3, $Mg(NO_3)_2 \cdot 6H_2O$, SnO_2, and Fe_2O_3. The mixtures were ground and pressed into pellets which were slowly heated to 1173 K and held there for 5 hr. The samples were then reground, repelleted, and fired at 1773 K for 4 hr for $Li_{2+x}(Li_xMg_{1-x}Sn_3)O_8$ compositions and at 1523 K for 15 hr for compositions $Li_2Mg_{1-x}Fe_{2x}Sn_{3-x}O_8$ with $x > 0$.

The materials were characterized by their X-ray powder patterns obtained at ambient temperature with a Guinier-Hägg camera, using Cu$K\alpha_1$ radiation and KCl as internal standard. A microdensitometer was used to obtain accurate d-spacings.

The impedance measurements were made on cylindrical disks ($\theta = 1.1$ cm, $l =$ 0.2–0.4 cm) sintered at the final firing temperatures. The density of the disks was estimated to be ~90% of the theoretical density. Blocking electrodes were applied by painting Engelhard gold paste onto the disk faces and heating them slowly to 673 K in order to decompose the organo-gold complex. The impedance of the disks was mea-

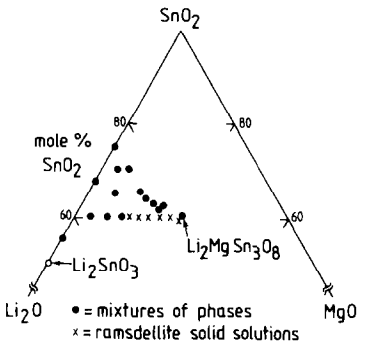

FIG. 3. Occurrence of ramsdellite solid solutions, $Li_{2+x}(Li_xMg_{1-x}Sn_3)O_8$ in the Li_2O–MgO–SnO_2 system at 1773 K.

sured using a Solartron 1172 FRA in the frequency range 1 Hz–10 kHz. In some cases the frequency range was extended to 1 MHz using a Wayne-Kerr B224 a.f. bridge for frequencies 100 Hz–50 kHz and a Wayne-Kerr B601 r.f. bridge for frequencies 50 kHz–1 MHz.

Results

$Li^c_{2+x}(Li_xMg_{1-x}Sn_3)^fO_8$ Ramsdellite Solid Solutions

A new range of ramsdellite-like solid solutions was synthesized in the system Li_2O–MgO–SnO_2 (Fig. 3). These extend from a composition at, or close to, $Li_2MgSn_3O_8$ in the direction of the hypothetical compound "$Li_4Sn_3O_8$," by means of the replacement mechanism $2\,Li^+ \rightleftharpoons Mg^{2+}$. The formula of the solid solutions may be written as $Li^c_{2+x}(Li_xMg_{1-x}Sn_3)^fO_8$: $0 \lesssim x \lesssim 0.5$.

X-Ray powder photographs showed that the materials deteriorate because of lithia loss when held at high temperatures for prolonged times as evidenced by the appearance and growth in intensity of lines from SnO_2. In order to obtain single phase samples of $Li_2MgSn_3O_8$ it was found necessary to add 10–15% extra Li_2CO_3 to the reaction mixture. No extra Li_2CO_3 was needed to prepare mono-phasic samples with $x \geq 0.1$. There is still, therefore, uncertainty as to whether stoichiometric $Li_2MgSn_3O_8$ exists as a stable phase (*2*).

The X-ray powder patterns of the new solid solutions were indexed on the basis of the orthorhombic ramsdellite unit cell. The lattice parameters were obtained from a least-squares refinement of the *d*-spacings and are given in Table II. The unit cell volume and *c*-axis show no substantial variation with composition while the *b*-axis decreases and the *a*-axis increases with increasing *x*. It is presumed that partial replacement of Mg^{2+} by Li^+ on octahedral sites does not cause major shifts in parameters, because of similar ionic radii of six-coordinated Li^+, 0.74 Å, and Mg^{2+}, 0.72 Å (*9*). The compositional dependence of *a* and *b* is thus probably caused by the change in Li^+ ion concentration and/or distribution in the ramsdellite channels with *x*.

$Li^c_2(Mg_{1-x}Fe_{2x}Sn_{3-x})^fO_8$ Solid Solutions

A series of solid solutions between the two ramsdellite end members, $Li_2MgSn_3O_8$ and $Li_2Fe_2Sn_2O_8$, was synthesized. To aid in the synthesis of single phase samples, it was found necessary to add 5% excess Li_2CO_3 to the reaction mixture for $x > 0$.

The lattice parameters of the solid solu-

TABLE II

LATTICE PARAMETER DATA

Composition	*a* (Å) ±0.001	*b* (Å) ±0.002	*c* (Å) ±0.001	*V* (Å^3)
$Li_{2+x}(Li_xMg_{1-x}Sn_3)O_8$				
$x = 0.0$	5.1008	10.0005	3.1092	158.60
$x = 0.1$	5.1038	10.0052	3.1104	158.83
$x = 0.2$	5.1274	9.9732	3.1028	158.67
$x = 0.3$	5.1271	9.9723	3.1044	158.72
$x = 0.4$	5.1408	9.9592	3.1041	158.92
$x = 0.5$	5.1536	9.9344	3.1021	158.82
$Li_2Mg_{1-x}Fe_{2x}Sn_{3-x}O_8$				
$x = 0.25$	5.0970	9.9646	3.0979	157.34
$x = 0.50$	5.0896	9.9293	3.0896	156.14
$x = 0.75$	5.0747	9.8989	3.0753	154.48
$x = 1.00$	5.0654	9.8683	3.0642	153.17
Polycrystalline $Li_2Ti_3O_7$ (*5*)	5.0163	9.5435	2.9452	141.00

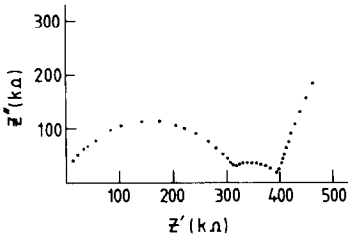

FIG. 4. Complex impedance diagram obtained at 406 K for composition $Li_{2.4}(Li_{0.4}Mg_{0.6}Sn_3)O_8$.

tions, Table II, show a liner decrease with x, reflecting the replacement of Mg^{2+}, Sn^{4+} ions by smaller Fe^{3+} ions. Lattice parameters for $Li_2Fe_2Sn_2O_8$ and $Li_2MgSn_3O_8$ are in good agreement with previously reported values (*1*, *2*).

Impedance Measurements

The impedance was measured as a function of frequency at an average of 12 temperatures per sample between 370 and 750 K and the data analyzed using the complex impedance formalism (*10*). The conductivities were determined from the intercept of the electrode polarization arc with the real axis in the complex impedance plane.

Compositions $Li_2Mg_{1-x}Fe_{2x}Sn_{3-x}O_8$ exhibited only one semicircle in the complex impedance plane. For $Li_{2+x}(Li_xMg_{1-x}Sn_3)O_8$ compositions with $x \geq 0.3$, there appeared at lower frequencies an additional smaller semicircle, $\sim\frac{1}{5}$ the size of the high frequency one. An example of a complex impedance plot showing two semicircles is given in Fig. 4. The parallel capacitances associated with the two semicircles were calculated to be ~7 and ~32 pF/cm, respectively. The relative sizes of the two semicircles did not vary with temperature. For this reason the second semicircle is believed to originate from constriction resistances between grains rather than from resistances of grain-boundaries with a different atomic structure.

In Fig. 5, $\log(\sigma T)$ is plotted versus $1/T$ for a selected number of $Li^c_{2+x}(Li_xMg_{1-x}Sn_3)^fO_8$ compositions. The Arrhenius curves for compositions with $x \geq 0.1$ show a rather small but significant curvature with higher activation energies in the middle part of the temperature range studied. The origin of the curvature is not clear; it may be an effect of highly anistropic conductivity in the grains of the polycrystalline samples. Arrhenius diagrams for compositions $Li_2Mg_{1-x}Fe_{2x}Sn_{3-x}O_8$ exhibited straight lines.

Activation energies, E_a, and preexponential terms $\log(\sigma_0)$, were obtained by fitting the conductivity data to the expression $\ln(\sigma T) = \ln(\sigma_0) - E_a/kT$ and are given in Table III.

The compositional variation of the conductivity for the $Li^c_{2+x}(Li_xMg_{1-x}Sn_3)^fO_8$ compositions is shown in Fig. 6. The conductivity increases as x increases from $x = 0$ and shows a maximum at $x = 0.3$. Compositions with $x \geq 0.3$ show a slight decrease in conductivity with increasing x.

In the $Li_2Mg_{1-x}Fe_{2x}Sn_{3-x}O_8$ series of compositions the highest conductivity is observed for $Li_2Fe_2Sn_2O_8$, $x = 1$.

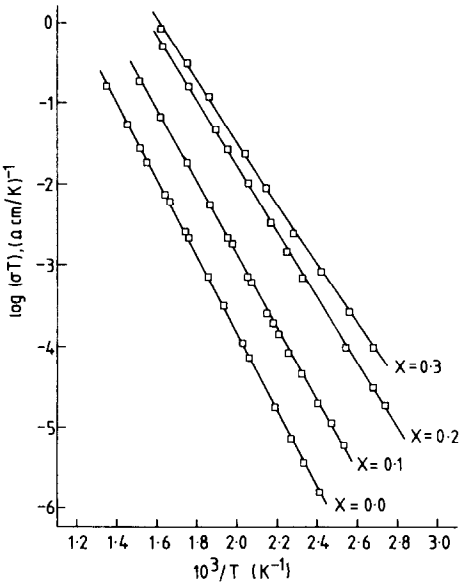

FIG. 5. $\text{Log}(\sigma T)$ versus reciprocal temperature for $Li_{2+x}(Li_xMg_{1-x}Sn_3)O_8$ compositions.

TABLE III
CONDUCTIVITY DATA

Composition	E_a (eV) error ± 0.02	log σ_0 (Ω cm/K)$^{-1}$, error ± 0.1	log σ (Ω cm)$^{-1}$ at 573 K
$Li_{2+x}(Li_xMg_{1-x}Sn_3)O_8$			
$x = 0.0$	0.93	5.50	−5.44
$x = 0.1$	0.89	6.04	−4.54
$x = 0.2$	0.79	6.19	−3.52
$x = 0.3$	0.74	5.99	−3.28
$x = 0.4$	0.76	6.11	−3.33
$x = 0.5$	0.78	6.25	−3.37
$Li_2Mg_{1-x}Fe_{2x}Sn_{3-x}O_8$			
$x = 0.25$	0.89	5.64	−4.95
$x = 0.50$	0.93	5.80	−5.14
$x = 0.75$	0.90	5.57	−5.10
$x = 1.00$	0.82	5.21	−4.76
Polycrystalline $Li_2Ti_3O_7$ (7)	0.46	4.24	−2.56

Discussion

The Li^+ ion conduction in the $Li_2Mg_{1-x}Fe_{2x}Sn_{3-x}O_8$ solid solutions is expected to be highly anisotropic. The occupancy of Li^+ ions in the framework sites of the ramsdellite double columns is nominally zero and the available pathways between adjacent channels are therefore restricted to be via the small tetrahedral B1 and B2 sites (cf. Fig. 1b). Such pathways appear to be energetically less favorable than the pathways available for Li^+ ion migration within the channels.

It is, however, conceivable that part of the excess lithia added during synthesis is incorporated into the structures, with consequent partial occupancy of Li^+ ions on octahedral E sites of the ramsdellite framework. This could then enable interchannel Li^+ migration to take place via the octahedral E sites. Alternatively, the double columns might also contain vacancies but this would imply that some of the higher valent metal ions were displaced onto interstitial positions within the channels.

The ionic conductivities of the $Li_{2+x}(Li_xMg_{1-x}Sn_3)O_8$ solid solutions can be compared with that of $Li_2Ti_3O_7$. Conductivity measurements on single crystals of $Li_2Ti_3O_7$ (*4*, *5*), showed that the activation energy is very nearly the same for conduction parallel to the three crystallographic axes, ~0.45 eV, and that $\sigma_c/\sigma_b \approx 7$, $\sigma_b/\sigma_a \approx 4$ at temperatures $290 \leq T \leq 770$ K. The conductivity is thus anisotropic but not sufficiently so for the material to be classified as a one-dimensional conductor. In $Li_2Ti_3O_7$ approximately 14% of the framework octahedral E sites are occupied by Li^+ ions (*3*). The Li^+ ions in the channels are found to be statistically distributed over two sets of tetrahedral sites, C1 and C4, near the center of the channels, at heights $\frac{1}{4}$ and $\frac{3}{4}$ along the *c*-axis (cf. Fig. 1c). The distance between two adjacent C1 and C4 sites at any one level along the *c*-axis is only ~0.9 Å and both such sites cannot therefore be occupied simultaneously by Li^+ ions. The average occupancy factor for Li^+ ions on individual C1 and C4 sites is ~43% and hence the occupancy of the levels is accordingly ~86%.

Crystallographic studies on $Li_2MgSn_3O_8$ have not been carried out and the following comments are based solely on lattice parameters and geometric considerations. In $Li_2MgSn_3O_8$, assuming a structure similar to $Li_2Ti_3O_7$, the framework octahedral E sites contain Mg^{2+} and Sn^{4+} ions only. The Li^+ ions then fully occupy the levels, at heights $\frac{1}{4}$ and $\frac{3}{4}$ along the *c*-axis, in the

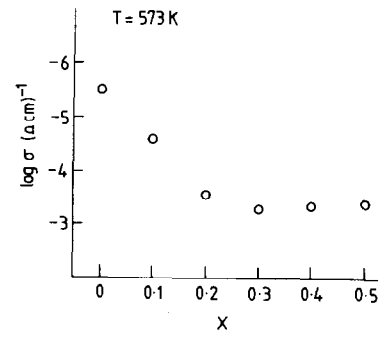

FIG. 6. The ionic conductivity at 573 K versus x in $Li_{2+x}(Li_xMg_{1-x}Sn_3)O_8$.

channels although at any one level they must occupy either a C1 or a C4 site. Since the relatively high conductivity and moderately low activation energy of $Li_2Ti_3O_7$ may be a consequence of the significant concentration of nonoccupied levels, then conversely the lower conductivity and higher activation energy of $Li_2MgSn_3O_8$ may be understood since these same levels are presumed full.

In the $Li^c_{2+x}(Li_xMg_{1-x}Sn_3)^fO_8$ solid solutions, the extra x Li^+ ions in the channel sites must presumably occupy a new set of sites, e.g., the C2 and C3 sites within the rectangular channels. As these sites are progressively occupied, with increasing x, so the conductivity increases and activation energy decreases. The structure and stoichiometry of $Li_2MgSn_3O_8$ may therefore represent a crossover between the Li^+ ion excess materials $Li_{2+2x}Mg_{1-x}Sn_3O_8$, and the Li^+ ion deficient $Li_2Ti_3O_7$, both of which are higher conductors than the "stoichiometric" parent phase, $Li_2MgSn_3O_8$.

An additional factor in the $Li^c_{2+x}(Li_xMg_{1-x}Sn_3)^fO_8$ solid solutions is that the occupancy of framework octahedral E sites by Li^+ ions nominally increases from zero for $x = 0$ to 12.5% for $x = 0.5$. The initial increase in conductivity with x may then also be due to an increasing number of pathways between channels, via E sites, as x increases.

The conductivity may also be influenced by the details of the oxygen ion arrangement and the overall cell dimensions. In the $Li_2Mg_{1-x}Fe_{2x}Sn_{3-x}O_8$ solid solution, the conductivity increases with x, accompanied by a decrease in lattice dimensions. The larger lattice size in the $Li_{2+x}Mg_{1+x}Sn_3O_8$ solid solutions, in comparison with $Li_2Ti_3O_7$, may then also cause the activation energies to be higher in the former.

Acknowledgment

J. Grins wishes to express his gratitude to I.C.I. for the fellowship in commemoration of Alfred Nobel which has made this study possible.

Note added in proof. Since this paper was prepared a note on the conductivity of $Li_2MgSn_3O_8$ has appeared (*11*). It has the value 2.3×10^{-4} ohm^{-1} cm^{-1} at 450°C with an activation energy of 0.76 eV over the temperature range 100 to 400°C.

References

1. J. Choisnet, M. Hervieu, B. Raveau, and P. Tarte, *J. Solid State Chem.* **40,** 344 (1981).
2. C. Keller and A. R. West, *J. Mater. Sci. Lett.* **2,** 451 (1983).
3. B. Morosin and J. C. Mikkelson, Jr., *Acta Crystallogr. Sect. B* **35,** 798 (1979).
4. J. B. Boyce and J. C. Mikkelsen, Jr., *Solid State Commun.* **31,** 741 (1979).
5. J. B. Boyce, J. C. Mikkelsen, Jr., and B. A. Huberman, *Solid State Commun.* **29,** 507 (1979).
6. A. M. Byström, *Acta Chem. Scand.* **3,** 163 (1979).
7. R. G. Wyckoff, "Crystal Structures," 2nd ed., Vol. I, p. 292, Wiley, New York (1963).
8. A. R. West and P. G. Bruce, *Acta Crystallogr. Sect. B* **38,** 1891 (1982).
9. R. D. Shannon and C. T. Prewitt, *Acta Crystallogr. Sect. B* **25,** 725 (1969).
10. I. M. Hodge, M. D. Ingram, and A. R. West, *J. Electroanal. Chem.* **74,** 125 (1976).
11. M. D. Lewis, N. Kimura, and M. Greenblatt, *J. Solid State Chem.* **58,** 401 (1985).